Spatiotemporal variation of rainfall over the central Himalayan region revealed by TRMM Precipitation Radar

Dibas Shrestha,[1] Prasamsa Singh,[2] and Kenji Nakamura[3]

Received 19 May 2012; revised 4 October 2012; accepted 5 October 2012; published 20 November 2012.

[1] The rainfall-elevation relationship in the central Himalayan region (CHR) for pre-monsoon and monsoon seasons is analyzed utilizing the 11-year (1998–2008) high-spatial-resolution TRMM PR 2A25 near-surface rainfall data. The results indicate a strong relationship between rainfall and elevation during both seasons. The investigation reveals a relatively large amount of rainfall over higher elevations during pre-monsoon season. Interestingly, two significant rainfall peaks appear over the southern slope of the Himalayas during summer monsoon season. The first primary peak appears along the Sub-Himalayas (~500–700 m above MSL), while the second appears along the Lesser Himalayas (~2,000–2,200 m above MSL). The former rainfall peak is attributed to fewer heavy rainfall events, and the latter to frequent, weak, but persistent rainfall. It is suggested that the atmosphere is insufficiently moist to trigger convections during the pre-monsoon season, and sufficiently moist during summer monsoon season. The convections over the Sub-Himalayas may moisten the middle layer, and the water vapor in the atmosphere condenses because of the forced lifting along the slope, forming the second rainfall band. The total rain amount is primarily determined by the frequency of rain. The rain-conditioned rain rate along the slope monotonically decreases with elevation. This shows that the precipitation occurs because of forced lifting. In addition, our results show that seasonal variation of rainfall is rather similar to the variation of rainfall characteristics observed during active and break periods.

Citation: Shrestha, D., P. Singh, and K. Nakamura (2012), Spatiotemporal variation of rainfall over the central Himalayan region revealed by TRMM Precipitation Radar, *J. Geophys. Res.*, *117*, D22106, doi:10.1029/2012JD018140.

1. Introduction

[2] The unique atmospheric uplifting of the massive Himalayan mountain system (Figure 1) modulates the climate of South Asia. Although the Himalayas play a vital role in the South Asian monsoon environment by guarding the Indian subcontinent from the dry, cold air masses of central Asia and blocking the warm, moist airflow from the Indian Ocean [e.g., *Barros et al.*, 2004; *Boos and Kuang*, 2010; *Flohn*, 1957], insufficient studies have been conducted over the Himalayan region because of a lack of adequate data [*Shrestha*, 2000]. Mountainous environments have a strong impact on spatial and temporal distribution of precipitation compared with the impact of plane areas. An important characteristic is the relationship between precipitation amount and elevation. Information on the variation of precipitation with elevation helps in providing a realistic assessment of water resources, estimation of maximum precipitation, and hydrological modeling of mountainous regions [*Barros et al.*, 2006]. In recent years, spatial variability in precipitation has received attention for studying the interactions among climate, erosion, and tectonics [e.g., *Anders et al.*, 2006; *Barros et al.*, 2006; *Bookhagen*, 2010]. Furthermore, it is hypothesized that an increase in rainfall variability in the Himalayan region is an important indicator of global climate change, because mountain environments are particularly vulnerable to such changes.

[3] In mountainous regions, orography provides necessary uplift to the air encountering mountains on windward slopes. Rising air cooled adiabatically results in increased relative humidity, which creates clouds and precipitation. This process is the main reason for increasing accumulated precipitation with altitude. Several studies have been conducted on the distribution of rainfall with elevation in various regions of the world [e.g., *Bookhagen and Burbank*, 2006; *Bookhagen and Strecker*, 2008; *Dairaku et al.*, 2004; *Dhar and Rakhecha*, 1981; *Linsley et al.*, 1949; *Rumley*, 1965; *Suprit and Shankar*, 2008], showing strong correspondence between rainfall and altitude. Using 50 rainfall stations, an attempt was made to ascertain the maximum elevation of increased rainfall

[1]Graduate School of Environmental Studies, Nagoya University, Nagoya, Japan.
[2]International Pacific Research Center, University of Hawai'i at Mānoa, Honolulu, Hawai'i, USA.
[3]Hydrospheric Atmospheric Research Center, Nagoya University, Nagoya, Japan.

Corresponding author: D. Shrestha, Graduate School of Environmental Studies, Nagoya University, Furo-cho, Chikusa-ku, Nagoya 464-8601, Japan. (st.dibas@yahoo.com)

0148-0227/12/2012JD018140

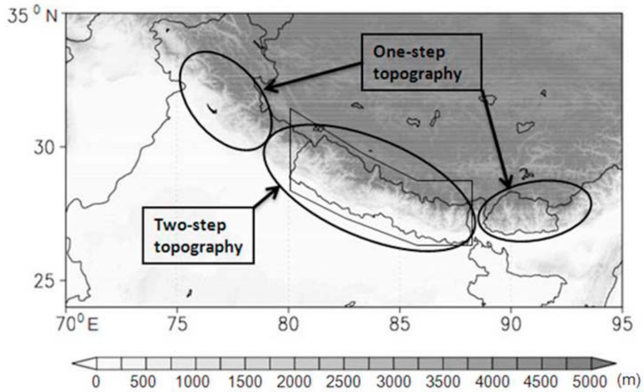

Figure 1. Topographic overview of the Himalayan range. International boarders are outlined in black. Eastern and western Himalayan regions are characterized by one-step topography; the central Himalayas are characterized by two-step topography. The area bounded by the thin black line represents the study area for statistical analysis.

in the central Himalayas during the monsoon season [*Dhar and Rakhecha*, 1981], showing that no linear relationship exists between rainfall and altitude and that the maximum rainfall zones fall near foothills at an elevation of 2.0–2.4 km. *Singh et al.* [1995] and *Singh and Kumar* [1997] also reported that there may be a continuous increase in precipitation with altitude in the western Himalayan region; however, precipitation begins to decrease above a certain altitude. A principle factor determining the relationship between precipitation amount and altitude is precipitation duration [e.g., *Dairaku et al.*, 2004; *Engman and Hershfield*, 1969; *Sokol and Bližňák*, 2009]. Previous studies have shown that rainfall amounts generally increase with altitude up to a certain height on windward slopes. However, this relationship varies considerably with time and place.

[4] Most of the previous studies on precipitation-altitude relationship were based on rain gauge data and were limited to basin scales. However, gauge networks are considered insufficient for vast mountain topography and are subject to various types of inaccuracies, such as measurement and representative errors. In this context, a broad picture of the relationship between precipitation and topography in the Himalayas can be derived from the precipitation radar (PR) onboard the Tropical Rainfall Measuring Mission (TRMM) [e.g., *Anders et al.*, 2006; *Barros et al.*, 2004; *Bhatt and Nakamura*, 2005; *Bookhagen and Burbank*, 2006, 2010; *Houze et al.*, 2007; *Nesbitt and Zisper*, 2003; *Romatschke and Houze*, 2011a, 2011b]. *Bookhagen and Burbank* [2006] analyzed TRMM 2B31 data product for eight years (1998–2005) to investigate the influence of topography and relief on rainfall generation and resultant erosion along the southern slope of the Himalayas. They discovered strong large-scale relationships among topography, relief, and rainfall location with two distinct rainfall maxima along two parallel topographical features. In the first case, an outer rainfall peak occurs in frontal regions throughout the Himalayas at an average elevation of ~0.95 km or a mean relief of ~1.2 km. In the second case, an inner band of rainfall typically peaks along the southern flank of the Greater Himalaya, particularly in the central region (~74°E–88°E) at an average ~2.1 km elevation or ~2 km mean relief. Moreover, *Bookhagen and Strecker* [2008] identified peak rainfall (>3.5 mm/h) at a mean elevation of 1.3 ± 0.17 km or a mean relief of 0.95 ± 0.08 km along the eastern flanks of the Andes, which is comparable to their observation in the Himalayas. Over high mountain barriers (e.g., Himalayas, Andes), maximum rainfall is generally caused by convection rather than topography in the mature monsoon season [*Romatschke and Houze*, 2011a; *Houze*, 2012]. Convections can occur when low-level warm moist airflow encounters hills near the base of major mountain ranges.

[5] Aside from seasonal variability, intraseasonal fluctuations (often referred to as active/break cycles) of rainfall in the summer monsoon season is a substantial component of the South Asian monsoon rainfall, because uneven spatial and temporal variation of rainfall during JJA may have an adverse effect on agriculture. The existence of active and break periods is caused by latitudinal oscillations of a monsoon trough. During active periods, a monsoon trough region extends from the head of the Bay of Bengal heat low over Pakistan along the Gangetic Plains. In contrast, a monsoon depression occurs close to the Himalayan foothills during break periods, where the southeasterly flow from the Bay of Bengal, and the southwesterly flow from the Arabian Sea branch meet and move northward [*Krishnamurthy and Shukla*, 2000; *Ramamurthy*, 1969]. The active monsoon rainfall is considered to be above normal over central India and below normal over the Himalayan foothills. This pattern is reversed during the break phase [*Krishnamurthy and Shukla*, 2000]. Several studies have described precipitation characteristics during active and break phases over central India and the Himalayan foothills [e.g., *Annamalai and Slingo*, 2001; *Singh and Nakamura*, 2010]. Subseasonal monsoon fluctuation is largely responsible for the spatial variation of rainfall over the southern slope of the Himalayas; however, no study has focused on each region to date. Information about variability in precipitation characteristics during active and break phases over the central Himalayan region (CHR) could improve understanding of Himalayan precipitation mechanisms.

[6] Therefore, the main objective of this study is to explore the impact of two-step topography in the CHR and the associated rainfall processes utilizing a high-spatial-resolution (~4 × 6 km) data set from TRMM PR 2A25 version 6. Although the data set provides observations at several altitudes, we mostly focus on near-surface rainfall, which is described in terms of rain frequency and conditional rain rate. To understand the precipitation scenario in the CHR, the summer monsoon rainfall mechanism is further explained in terms of the Himalayan active and break periods (also known as wet and dry periods).

[7] This paper is arranged as follows: section 2 presents the data and methodology; section 3 provides topographic information about the Himalayas, particularly in the CHR; section 4 gives the results of TRMM-PR observation; section 5 discusses possible mechanisms; and section 6 summarizes our findings.

2. Data and Methodology

[8] In this study, the TRMM satellite's PR version 6 products have been processed for pre-monsoon (March–May;

MAM) and summer monsoon (June–August; JJA) for 1998–2008 for use as primary data. Briefly, TRMM PR is the first spaceborne radar designed to provide three-dimensional maps of storm structures [*Kummerow et al.*, 1998, 2000]. PR has horizontal resolution of $\sim$4 $\times$ 6 km and vertical resolution of 250 m at nadir with 215-km swath width operating at 13.8 GHz. It can detect reflectivities down to nearly 17 dBZ, equivalent to rain rates of $\sim$0.5 mm/h. The pixel size, swath width, and sensitivity to rain changed slightly (5-km pixel size, 247-km swath width and sensitivity reduced by 1.2 dB) after an orbit boost from 350 km to 402.5 km in 2001. However, the differences are insignificant and are neglected in this study. To study rainfall patterns, product 2A25 [*Iguchi et al.*, 2000] was used; it provides near-surface rain rate from PR. "Near-surface" rain rate was obtained from the range bin closest to the surface that is generally not corrupted by surface clutter. The near-surface height ranged from 500 m above ground level (AGL) at nadir to 2000 m AGL at the edge of the observation swath. The average rain rate is calculated as a product of rain frequency (number of rain samples normalized by total number of samples) and conditional rain rate (near-surface rain rate only when it is raining). The storm height data were obtained from PR product 2A23. The TRMM 2A23 storm height product is based on the 18-dBZ (equivalent to approximately 0.5 mm h^{-1}) echo-top height. Storm height was calculated only when it was raining. For data processing, instantaneous data were gridded at a grid size of 0.1° $\times$ 0.1° for 24, 1-h intervals; this is almost double the PR pixel size of 0.05°.

[9] We used TRMM PR product 2A25 for rain-type classifications (copy of the 2A23 rain type field). The PR algorithm classifies the rain pixels into three categories: convective, stratiform, and others. This classification is based on the vertical pattern of the profile (known as the V-method [*Awaka et al.*, 1997]) and on the horizontal variability of the echo (known as the H-method [*Steiner et al.*, 1995]). In brief, when a bright band is detected near the freezing level, the precipitation is classified as stratiform. If a bright band is not detected, and the maximum value of radar reflectivity in the beam exceeds 39 dBZ, rain type is classified as convective. When the precipitation type is neither stratiform nor convective, it is labeled as "other." The "other" category represents either noise or regions of precipitation aloft with no precipitation near the surface.

[10] There have been several studies on active and break monsoon based on different criteria and locations [e.g., *Annamalai and Slingo*, 2001; *Gadgil and Joseph*, 2003; *Krishnan et al.*, 2000; *Rajeevan et al.*, 2010; *Webster et al.*, 1998]. Traditionally, active and break periods have been identified on the basis of surface pressure and wind patterns over the Indian region [e.g., *Dhar et al.*, 1984; *Ramamurthy*, 1969; *Webster et al.*, 1998; *Goswami and Ajaya Mohan*, 2001]. In several recent studies [e.g., *Annamalai and Slingo*, 2001; *Gadgil and Joseph*, 2003; *Rajeevan et al.*, 2010; *Singh and Nakamura*, 2010], "breaks" (and active spells) are defined in terms of the rainfall over the monsoon zone during the mature monsoon months July–August. A different approach [*Krishnan et al.*, 2000] used outgoing longwave radiation (OLR), which is a proxy for rainfall, to define breaks. In this study, we used the TRMM 3B42 version 6 daily rainfall data for the 11-year period to identify active and break periods. TRMM 3B42 provides fine scale (0.25° $\times$ 0.25°, 3 hourly) data in a global belt extending from 50°S to 50°N latitude [*Huffman et al.*, 2007]. This product combines PR, multisatellite passive microwave, and geostationary infrared rainfall estimates. The criteria defined by *Singh and Nakamura* [2010] were adopted to identify active- and break-monsoon periods but for different locations. This criteria defines active (break) phases when daily rainfall over the Himalayan foothills (82°E–86°E, 27°N–28.5°N and 86°E–90°E, 26°N–27°N) is more (less) than 0.5 standard deviations from the average of July–August for each year for a minimum of three consecutive days. The numbers of active and break days using our criteria were 83 and 144, respectively. In general, these active and break days were consistent with those identified by *Singh and Nakamura* [2010], although different locations were chosen for the study. Active and break spells existed in almost every monsoon; only one season (1999) did not have any active events. An average of 7.55 active and 13.09 break days was observed during July–August. Most of the active spells lasted 3–4 days, while more than 50% of the dry spells were of such duration.

[11] For statistical analysis of altitudinal variations, precipitation characteristics were averaged for each 200-m altitude interval up to 5,000 m. The analysis was restricted within 5,000-m elevation because some of the highest altitude pixels showed excessively high magnitudes of rainfall. For example, pixels that include the world's highest peaks, Mt. Everest (8,848 m), Mt. Lhotse (8,516 m), and Mt. Cho Oyu (8,188 m), exhibited high rainfall totals of 4.95 mm/d. These high totals could be attributed to ground clutter contamination in radar echoes. Ground clutter occurs because of radar returns from higher terrain being misread as reflectivity owing to raindrops. Such contamination is more likely over steep slopes. This is because chances of reflection of the beam increase in areas of steep slope, as the incidence angle of the beam increases [*Anders et al.*, 2006]. The effect of ground clutter contamination on the representation of spatial pattern of rainfall is small over lower elevation mountainous regions [*Anders et al.*, 2006; *Takahashi et al.*, 2010]. Another reason to limit the area to altitudes below 5000 m elevation is simply to exclude the northern slopes of the Himalayas. The averaged values were smoothed by a 1:2:1 smoothing filter. Smoothed values (SV) are given as

$$SV_a = \frac{V_{a-1} + 2V_a + V_{a+1}}{4},$$

where V and a represent the averaged value and altitude, respectively.

[12] One of the major issues in satellite-based rainfall products is the estimation of sampling error. This is because a low earth orbit satellite is unable to provide continuous coverage of a given area. For a small number of samples, sampling error is likely to be more significant than retrieval error [*Bell and Kundu*, 2000]. Several researchers suggest that TRMM PR sampling errors are small ($\sim$10%) for monthly rainfall totals [*Anders et al.*, 2006; *Bell and Kundu*, 2000]. In this study, we compared results for the first half (1998–2004) and second half (2004–2008) of the study periods to check the consistency of our findings. Figure 2 illustrates the spatial variation of rainfall across the central Himalayas (84.5°E–85.0°E, 26.0°N–30.0°N) for MAM and JJA. During MAM

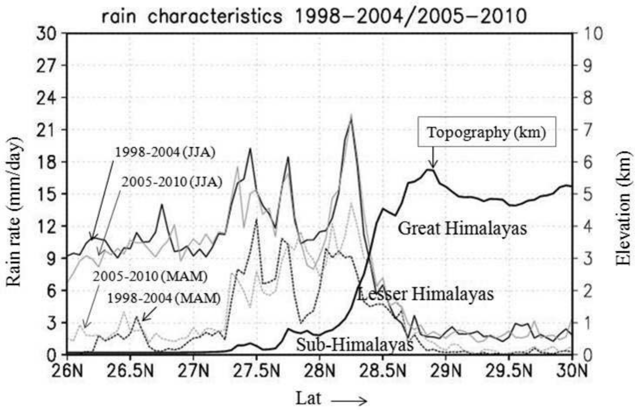

Figure 2. Rain rate distribution across the central Himalayas (84.5°E–85.0°E, 26.0°N–30.0°N) during pre-monsoon (MAM, dotted lines) and summer monsoon (JJA, solid lines) seasons for the first half (1998–2004, black lines) and second half (2005–2010, gray lines). Bold, heavy line represents topography for the same location.

and JJA in both halves of the study period, general patterns of rainfall are similar. This comparative analysis confirmed the consistency of basic findings.

[13] In addition to TRMM PR data, we used reanalysis data from the Japanese 25-year reanalysis project (JRA-25) on a 0.5° × 0.5° grid [*Onogi et al.*, 2005], which provided data to study the relationship between rainfall distribution and large-scale atmospheric circulation. Reanalysis data for the South Asian continent were taken from the 30-year period from 1979 to 2008 for MAM and JJA.

[14] The GTOPO30 data set of the United States Geological Survey (USGS) with a spatial resolution of 0.008° × 0.008° was used for topographic data analysis. For this study, data were averaged over 0.1° × 0.1° grids.

3. The Central Himalayan Region

[15] Distinct topographic patterns exist in the Great Himalayas (Figure 1). The eastern and western Himalayas are characterized by one-step topography [*Bookhagen and Burbank*, 2006, 2010], i.e., the Himalayas without its subordinate Himalayas, with consistent increment in elevation. In contrast, the central region is characterized by two-step topography, i.e., topography that includes the major Himalayas and their subordinate Himalayas. Note that the major Himalayas consist of the Lesser Himalayas and Greater Himalayas, and the subordinate Himalayas indicate the Sub-Himalayas (Figure 2).

[16] The study area (outlined by the thin black rectangle in Figure 1) covers approximately 1,000 km and includes the most rugged portion of the complex Himalayan topography (approximately 2,400 km). The highly elevated central Tibetan Plateau is located to the north and the low-elevation Gangetic Plains to the south. The CHR is located approximately on the margin of 26.0°N–31.0°N, 80.0°E–88.5°E in South Asia. East of 84.0°E, the mountains run roughly in an E–W direction; to the west of 84.0°E, the mountain range is oriented in an ESE–WNW direction. The range is characterized by narrow and sharply uplifted topography from south to north with a remarkable arrangement of parallel mountain chains. Elevation varies from approximately 60 m above mean sea level (AMSL) in the southern (Terai) plane to 8,848 m (Mt. Everest) in the northeast within a few tens of kilometers. Such extreme variation in altitude leads to a wide range of climatic conditions. Within the Himalayas, climate varies depending on elevation and location: the climate ranges from tropical at the base of the mountains to cold alpine at the highest elevations.

[17] Physically, the CHR forms three sub-parallel zones: the Greater Himalayas (GH), the Lesser Himalayas (LH; also known as the Mahabharat Range), and the Sub-Himalayas (SH; known as the Siwalik Range). The parallel ranges may exert a significant influence on monsoon and rainfall pattern [e.g., *Anders et al.*, 2006; *Bookhagen and Burbank*, 2006, 2010]. The SH (~500–1,200 m AMSL) is the southernmost mountains in the Himalayan range, which is considered to be the first zone of heavy rainfall in JJA. The LH (1,200–3,000 m AMSL) is located between the SH and GH, where rainfall activity is more concentrated. Small valleys are oriented in the E–W direction between the SH and LH. The GH (over 3,000 m AMSL) is located north of the LH, and is characterized by less rainfall activity; however, the region experiences significant snowfall during winter.

4. Results

4.1. Spatial Distribution of Rainfall

[18] First, we examined the spatial and temporal distribution of the rainfall around the Himalayas for MAM and JJA. Monthly average rainfall (expressed in mm/d) over 11 years (1998–2008) is shown in Figure 3, which indicates a clear contrast in horizontal distribution and magnitude of rainfall between MAM and JJA. It was observed that the greatest amount of rainfall occurred in JJA over the eastern Himalayan region and CHR. *Bookhagen* [2010], *Bookhagen and Burbank* [2010], and *Nayava* [1980] also noted that summer monsoon rainfall provides more than 80% of the annual moisture budget for the CHR. A clear double band of rainfall maxima exists in JJA, but is absent in MAM over the CHR (Figure 3a). Interestingly, high rainfall was observed in the higher terrain over the CHR in MAM. During JJA, a distinct feature of rainfall distribution was observed in the eastern, central, and western Himalayan regions (Figure 3b). The eastern and western regions displayed a single zone of rainfall maxima; the eastern region showed high rainfall over lower elevation areas (below ~1,000 m AMSL); conversely, the western region exhibited high rainfall over higher elevation areas (above ~1,000 m AMSL). Previously, *Bookhagen and Burbank* [2006, 2010] found rainfall pattern in the eastern and western Himalayas to be characterized by singles peak over low-altitude areas. In contrast, the central region exhibited two zones of rainfall maxima. A comparatively narrow and continuous peak rainfall band appeared along the front of the low-elevation mountain range and a discontinuous and relatively broader band occurred along the steep slope of the LH. These results are consistent with those of *Bookhagen and Burbank* [2006, 2010], who noticed double bands of rainfall maxima in the annual rainfall total.

[19] Next, we examined storm height distribution over the Himalayas (Figure 4). The actual storm height presented here corresponds to the height of the top of the precipitation column above ground level rather than AMSL. The

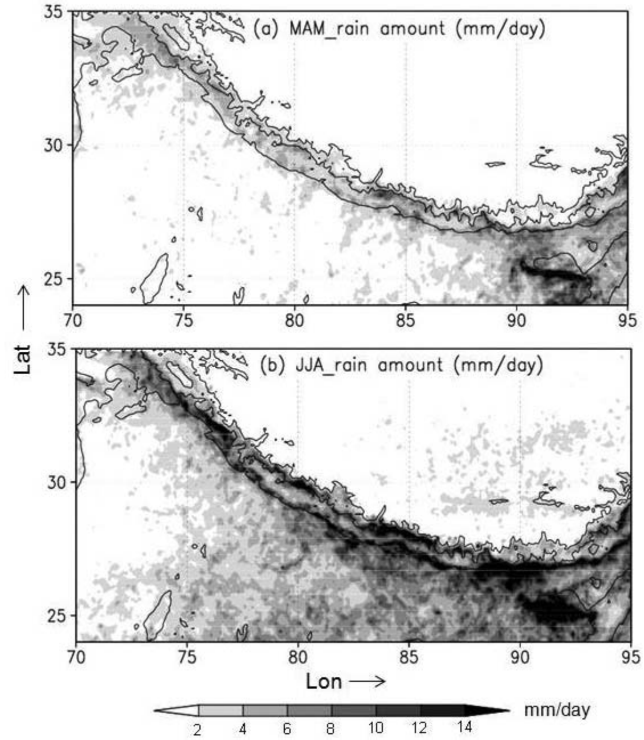

Figure 3. Distribution of rainfall amount in the 11-year period (1998–2008) in mm/day for (a) pre-monsoon (MAM) and (b) summer monsoon (JJA). Contour lines indicate 500, 2000, and 4000 m elevations.

correspondence between storm height and topography was clear in the eastern and western Himalayas, where tall storms were observed over low-altitude areas (Figure 4a) in MAM. Over the CHR, storms were found to be shallow and disorganized. Compared with MAM, topography-dependent storms were noticed over the entire Himalayan region in JJA (Figure 4b), which may indicate a less convective rain system in JJA. Results suggest that storms are shallow over higher elevation areas in JJA over both the eastern and central Himalayas, whereas a wide area of tall storms from lower to higher elevations were observed in the foothills of the western Himalayas. These tendencies are consistent with the occurrence of deep and wide intense convective processes in the western Himalayas and with wide convective and broad stratiform systems at the lower elevations of the central and eastern Himalayas [*Houze et al.*, 2007]. An example of latitudinal variation of storm height during MAM and JJA in the central Himalayas is shown in Figure 4c. General patterns of storm height distribution are similar during both seasons. The storm height was about 6 km AMSL with a clear peak near the top of the slope and a small peak at the bottom. Note that there is less latitudinal variability of storm height with a relatively smaller standard deviation in the summer monsoon season compared with the pre-monsoon season.

[20] A considerable amount of spatial and temporal variability in the rainfall distribution around the Himalayas was noted. Some studies [e.g., *Bookhagen and Burbank*, 2006, 2010] explained that spatial variability in JJA is greatly attributed to the distinct topography of the Himalayas. The CHR comprises a frontal low-altitude mountainous range and inner major mountain topography. As evident in our results, the double bands of rainfall maxima correspond to these two significant rises in topography, particularly in JJA. Thus, the spatiotemporal variations of rainfall and their mechanisms are likely to differ from other regions of the Himalayas.

[21] We now focus on unique features of the spatiotemporal variation of rainfall in the CHR. Essentially, the lower and higher elevation areas mentioned in this study refer to the zones of the primary rainfall peak along the SH and the secondary rainfall peak in the LH, respectively.

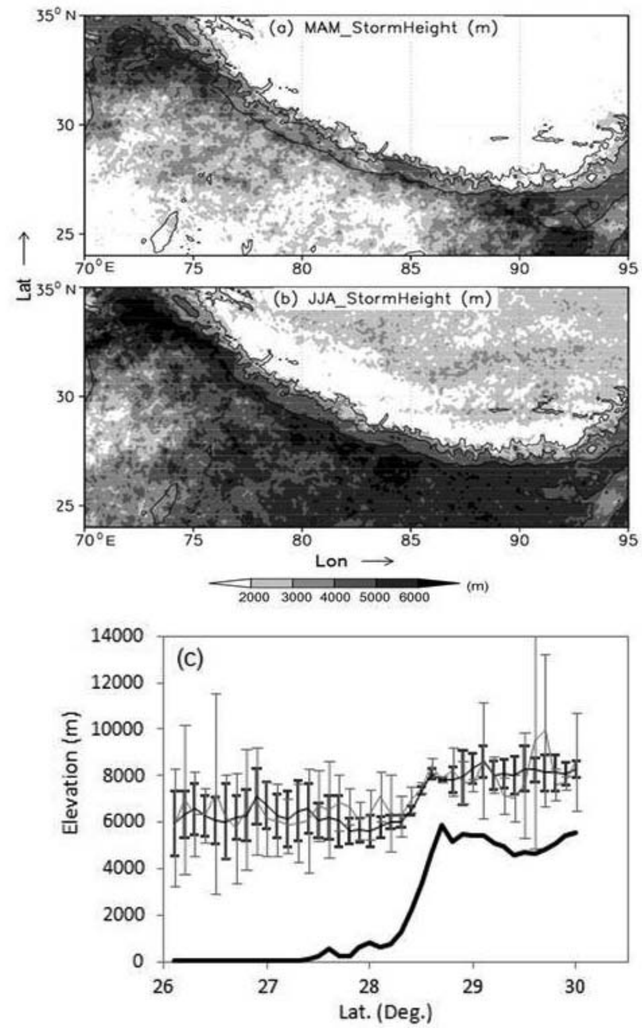

Figure 4. Horizontal distribution of actual storm height for (a) pre-monsoon (MAM) and (b) summer monsoon (JJA). Storm height (m) is calculated above the ground level instead of the sea level. (c) Mean storm height (above mean sea level) distribution across the central Himalayas (84.5°E–85.0°E, 26.0°N–30.0°N) with standard deviation plotted (shown by error bar) during MAM (gray line) and JJA (black line). Bold solid line represents topography for the same location. Contour lines represent 500, 2000, and 4000 m elevations.

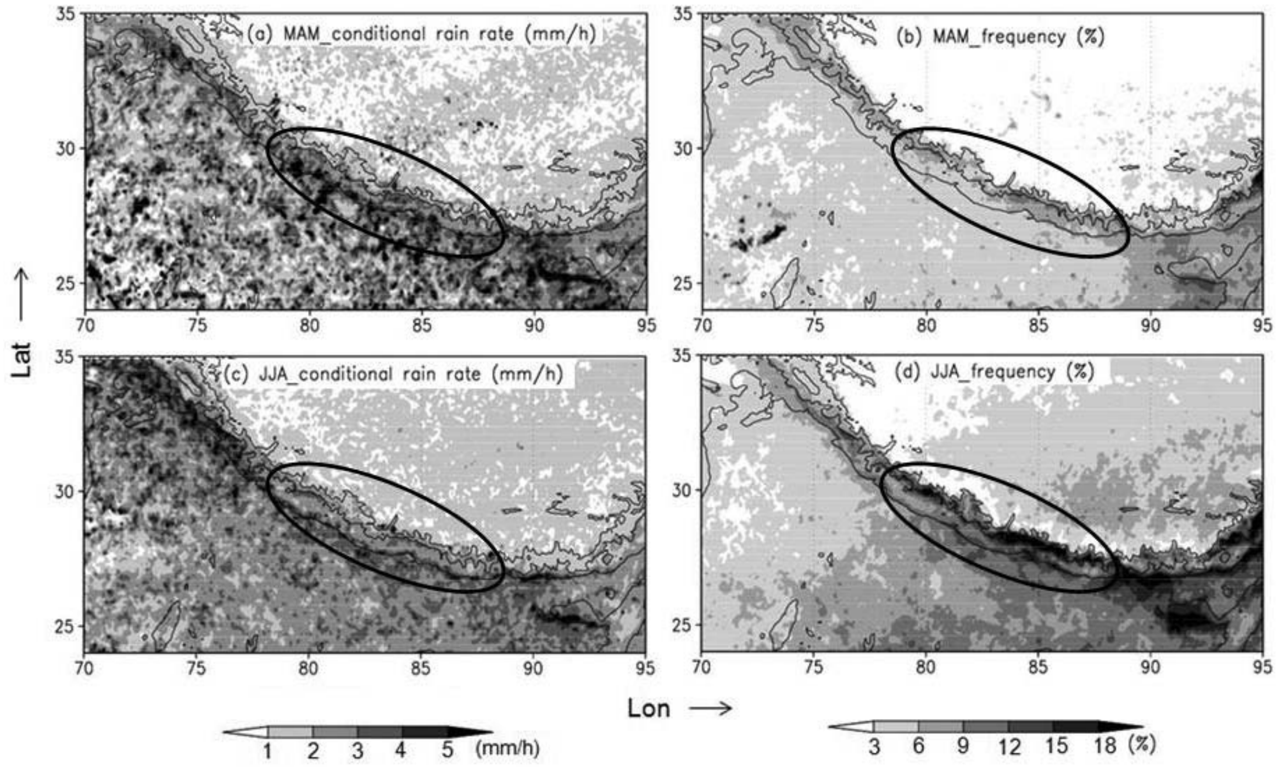

Figure 5. Horizontal distribution of rainfall characteristics for pre-monsoon (MAM) and summer monsoon (JJA). (a) Conditional rain rate for MAM (mm/h), (b) frequency of rainfall for MAM (%), (c) conditional rain rate for JJA (mm/h) and (d) rain frequency (%) for JJA. The area enclosed by the black oval lines represents the central Himalayan region (CHR).

4.2. Rainfall Frequency and Conditional Rain Rate

[22] Most of the previous studies have investigated only climatological mean rainfall patterns. However, it is unclear whether the amount of rainfall is caused by a larger number of weaker rainfall events or a smaller number of stronger rainfall events. The differences should be a reflection of the precipitation mechanism, which is an interesting subject for research. In addition, such differences are relevant to society; for example, strong but rare precipitation tends to cause more damage. Therefore, we discuss the rainfall frequency, conditional rain rate, and vertical structure of rainfall in this section.

[23] In MAM, the conditional rain rate was approximately 3–5 mm/h (Figure 5a), which is slightly higher than or equal to that in JJA (Figure 5c); however, the frequency was remarkably lower in MAM (Figures 5b and 5d). Hence, less frequent rainfall activity can be considered a cause of the rainfall minima in MAM. Over the LH, rain frequency was approximately 6–12%, which is two times as frequent as that rain over the low-elevation areas. Although a high conditional rain rate appeared over low-altitude areas, a smaller amount of rainfall was observed, suggesting that the higher elevation area received a larger amount of rainfall caused by a higher frequency of rainfall. In JJA, the conditional rain rate was greater than 3 mm/h and the frequency of rainfall was approximately 9–12% in lower elevation areas, while the conditional rain rate was less than 3 mm/h and the frequency of rainfall was approximately 12–18% over higher elevation areas. These findings indicate that the rainfall maxima over higher elevation areas are the result of a higher frequency of rainfall and that those over lower elevation areas are the result of both high conditional rain rate and high rain frequency. These findings agree well with the results of *Dairaku et al.* [2004] based on the data obtained from 15 rainfall stations in the Mae Chaem watershed, Thailand.

[24] To more precisely quantify the relationship between rainfall characteristics and altitude, we analyzed area-averaged total rainfall, rain frequency, and conditional rain rate over the southern slopes of the Himalayas up to 5,000 m elevation. Averaged values of all three components for each 200-m elevation area are presented in Figure 6. No clear rainfall peak was evident in MAM, although a slightly higher broad peak was observed over higher altitude areas (Figure 6a). This feature is different than that typically observed in JJA periods. The two rainfall peaks, previously observed by *Bookhagen and Burbank* [2006], have been observed in JJA. The primary peak of total rainfall appeared at a mean elevation of 500 m (AMSL) and the secondary peak appear at a mean elevation of 2,100 m (AMSL) (Figure 6b). The figure shows that the conditional rain rate decreases as altitude increases, whereas the frequency of rainfall increases as elevation increases, up to a certain altitude. These results demonstrate that the high-altitude rainfall peak is followed by more frequent rainfall rather than a high conditional rain rate.

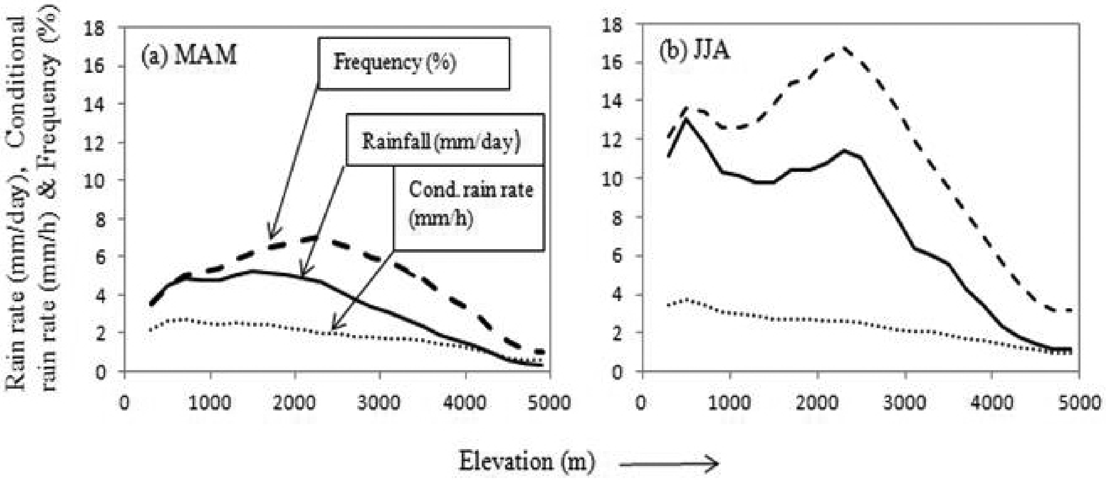

Figure 6. Variation of rainfall characteristics (rainfall, conditional rain rate, and rain frequency) with elevation for (a) pre-monsoon (MAM) and (b) summer monsoon (JJA). Solid, dotted, and dashed lines represent daily rainfall total (mm/day), conditional rain rate (mm/h), and frequency of rainfall (%), respectively.

Despite fewer rainfall events, a low-altitude primary rainfall peak was noticed, which indicates that strong rainfall events contribute to a larger amount of rainfall over lower elevation areas.

[25] Figure 7 depicts the vertical cross section of rain rate during MAM and JJA. That storm top reached above 12 km in height suggests a deep convective system, particularly over the SH and the southern plains in MAM (Figure 7a). The tall storm height in the CHR is consistent with *Romatschke and Houze*'s [2011b] finding of more convective-type rainfall during pre-monsoon in the central Himalayan foothills. In JJA, rain-top height is lower and more homogeneous (Figure 7b). Such patterns in storm height suggest that there is pronounced persistent rainfall and this could cause higher total rainfall. Compared with the low-altitude regions, the high-altitude regions experience lower rain-top height.

4.3. Rain-Type Distribution

[26] Mountains can generate both stratiform precipitation, which occurs in a statically stable atmosphere, and convective precipitation, which results from the release of static instability. Thus, considerable spatiotemporal variation in rain type is also expected over the CHR. Information about rain-type distribution could provide valuable insight into rain systems. Pre-monsoon rain systems are most convective, whereas summer monsoon systems are more stratiform in the CHR [*Romatschke and Houze*, 2011b]. Figure 8a shows the difference in the conditional rain rate between stratiform and convective rain in JJA. Relatively larger and smaller differences were detected in the low- and high-terrain areas, respectively, which suggests a strong convective rain over the frontal low-altitude topography. Similarly, the difference

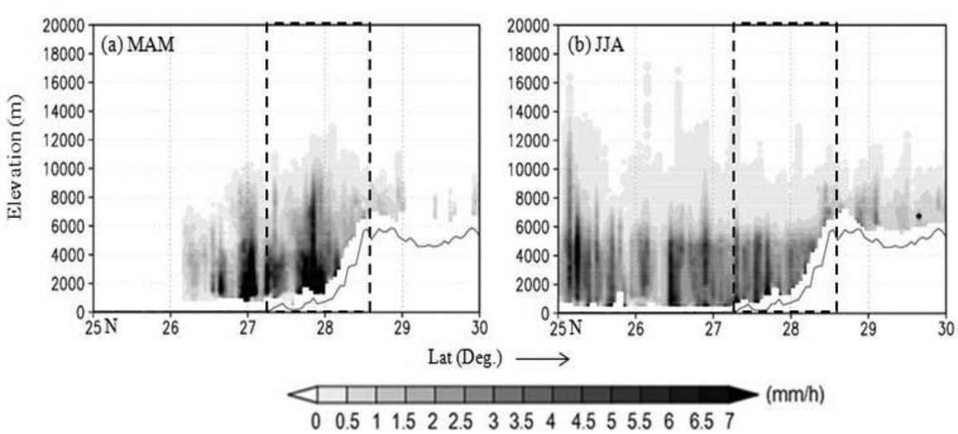

Figure 7. Vertical structure of rainfall (mm/h) at 84.5°E for (a) pre-monsoon (MAM) and (b) summer monsoon (JJA). Dashed rectangle indicates cross section of study area over the southern slopes of the Himalayas. Gray line represents north-south Himalayan topography at the same location.

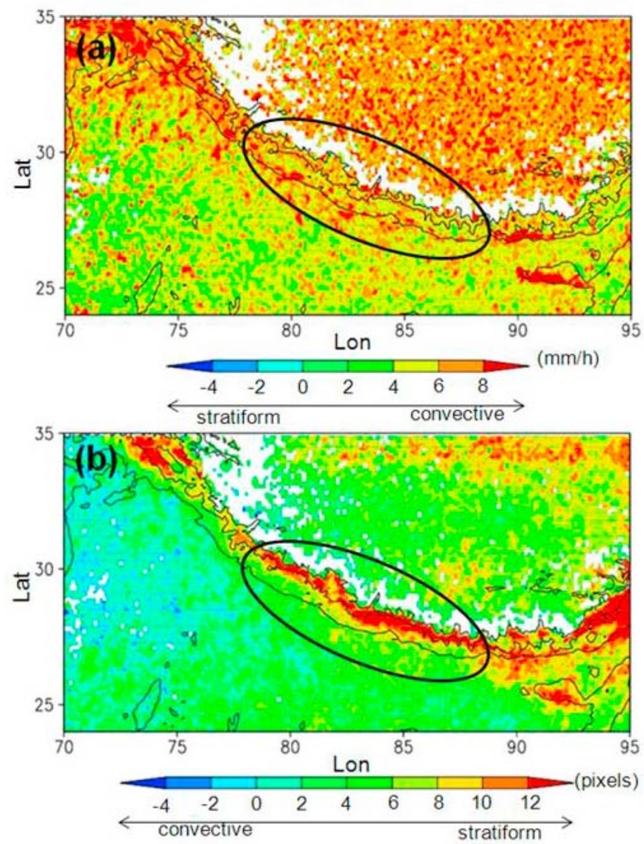

Figure 8. Horizontal distribution of rainfall types during summer monsoon (JJA). (a) Difference between the convective and stratiform rain rates (mm/h), and (b) difference between the occurrence of stratiform and convective rainfall events. The area enclosed by the black oval lines represents the central Himalayan region (CHR).

in the occurrence of stratiform and convective rain events (number of stratiform/convective rain pixels) is shown in Figure 8b. A large difference appeared over the higher elevation area, indicating that the maximum number of stratiform rainfall events occur over higher terrain. Furthermore, an area-averaged analysis of rain-type characteristics in JJA showed a linear increase in the occurrence of stratiform rainfall as altitude increases up to 2,200 m elevation (Figure 9a), inferring that an area of high-rainfall frequency coincided with an area of active stratiform rainfall. This tendency is consistent with the higher percentage of convective rain over lower terrain, and more stratiform rain over higher terrain [*Romatschke and Houze*, 2011a]. In conclusion, higher topography favors frequent but less intense stratiform rainfall, which leads to rainfall maxima in the LH, whereas lower terrain receives high rainfall amounts as a result of strong convective rainfall (Figure 9b).

4.4. Active- and Break-Period Rainfall Distributions

[27] MAM is characterized by a dry atmosphere compared to that of JJA. The seasonal variation described in the previous section may be similar to the variation in active and break periods in the mature monsoon season. Thus, we examined the variation of rainfall characteristics during active and break periods.

[28] The composite map of wet and dry phases for 11 consecutive summers over the Himalayas is similar to that of *Singh and Nakamura* [2010] (figure not shown). During active periods, rainfall increased around the southern slopes of the Himalayas and decreased over Indian plains, particularly over central India. In contrast, the opposite scenario occurred during dry periods. More interestingly, distinct features were observed even within the southern faces of the CHR and their surroundings during active and break phases. A high amount of rainfall was recorded only during active periods over the Himalayan foothills; however, higher elevation areas apparently experienced high rainfall even in dry periods. The high rainfall during active periods tends to be more persistent with lower echo-top height in the SH than in the LH (Figure 10a). Overall, the rainfall during the active period has higher echo-top than that during the break period (Figure 10b). The lowering of the echo-top height in the break periods may be because of the greater number of shallow convective storms [*Singh and Nakamura*, 2010].

[29] Details of statistical outputs of altitudinal patterns of rainfall characteristics are presented in Figure 11. During active periods, the daily rainfall reached 24 mm/day over the SH, which is significantly higher than the mean monsoon daily rainfall (∼13 mm/day), whereas much less rain (∼5 mm/day) was observed during the break period

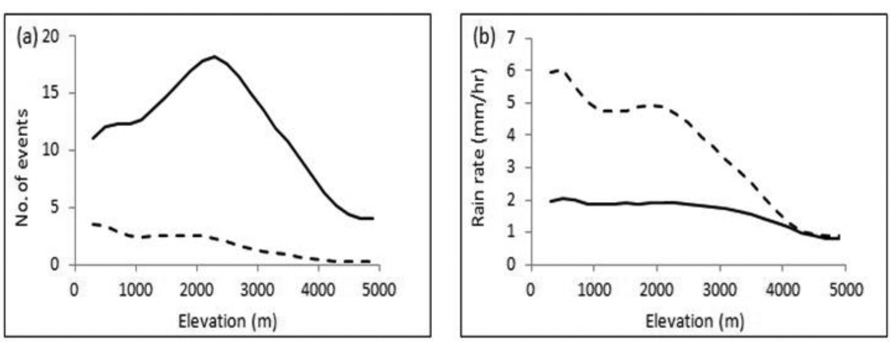

Figure 9. Altitudinal variation in rain type during summer monsoon (JJA) for (a) occurrence of rain events (pixel) and (b) rain rate (mm/h). Solid and dashed lines indicate stratiform rainfall and convective rainfall, respectively.

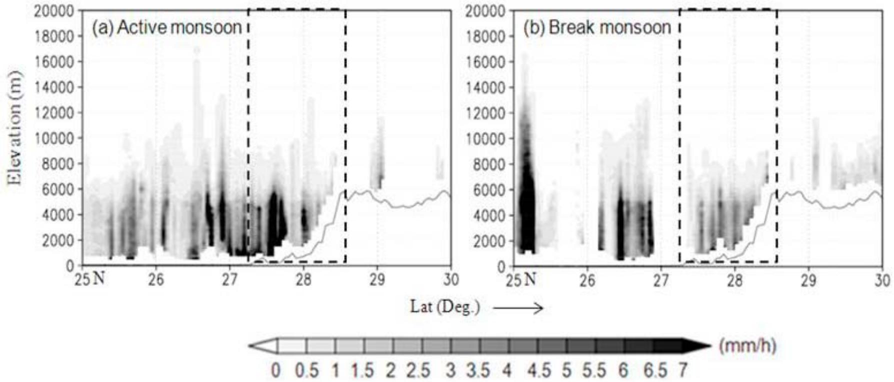

Figure 10. As in Figure 7, but for (a) active monsoon and (b) break monsoon.

(Figure 11a). On the contrary, no significant difference was detected in rain totals over the LH. A prominent feature in total rain distribution is the linear decrease (increase) during the active (break) period up to a certain altitude, which implies that the rainfall amount over the SH was mostly dependent on active-period rainfall; however, both periods affected the LH. Further, these results confirm that there are fewer rainy days in low-altitude regions than in higher altitude regions. The percentage of active- and break-periods rain was investigated to observe the contribution of active and break period rainfall to overall mature monsoon rainfall (Figure 11b). The "percentage of rain" was defined as the percentage of total rainfall amount in active/break period to summer monsoon rainfall total. Our observations suggest that the active-phase rainfall was dominant (>20%) in JJA rainfall total over the SH. However, on an average, there were fewer active days (7.55 days) than break days (13.09 days). In contrast, break-period rainfall was dominant above 1,700 m elevation. Figure 11c shows the altitudinal variation of the rain-conditioned rain rate for active and break periods. The patterns for both were similar; that is, heavy rainfall occurred over low-altitude regions and decreased with increasing altitude. Figure 11d shows the altitudinal variation of rain frequency for active and break periods. During active periods, a peak appears over the southern slope of the SH; during break periods, a broad peak is observed over the LH. These patterns are exactly to the same as those of the rain rate. Thus, it is suggested that rain frequency is mainly responsible for altitudinal variation of rainfall over the Himalayas during both periods. In summary, the general pattern of active- and break-phases rainfall characteristics was similar to that observed in the summer monsoon and premonsoon seasons.

4.5. Atmospheric Conditions

[30] Here, we discuss the vertical cross section of atmospheric circulation during MAM and JJA. Convective activity due to orographic lifting is an important factor in the generation of rainfall over mountains [*Chater and Sturman*, 1998]. The variation in equivalent potential temperature (commonly referred to as theta-e, i.e., θ_e) with height (600–925 hPa) over the area of interest (areas in rectangles Figures 12 and 13) was used to understand the strength of atmospheric instability (AI). The climatology of the atmospheric vertical structure from the

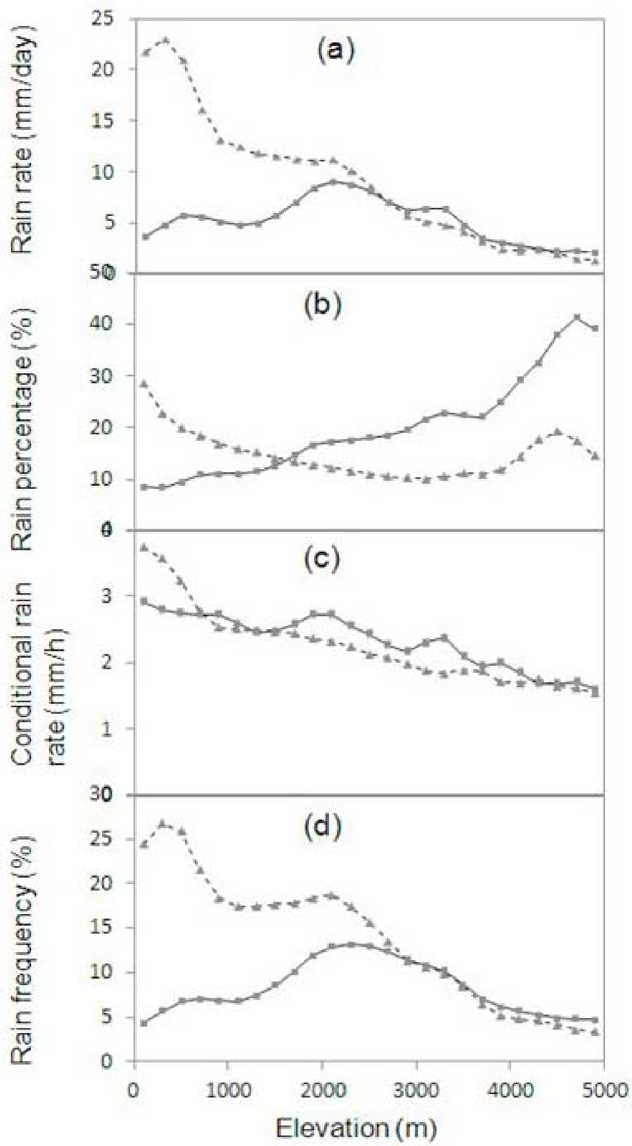

Figure 11. Altitudinal variation in rain characteristics during active (dashed line) and break (solid line) periods for (a) rain total (mm/day), (b) active/break rain percentage (%), (c) rain-conditioned rain rate (mm/h), and (d) frequency of rain (%).

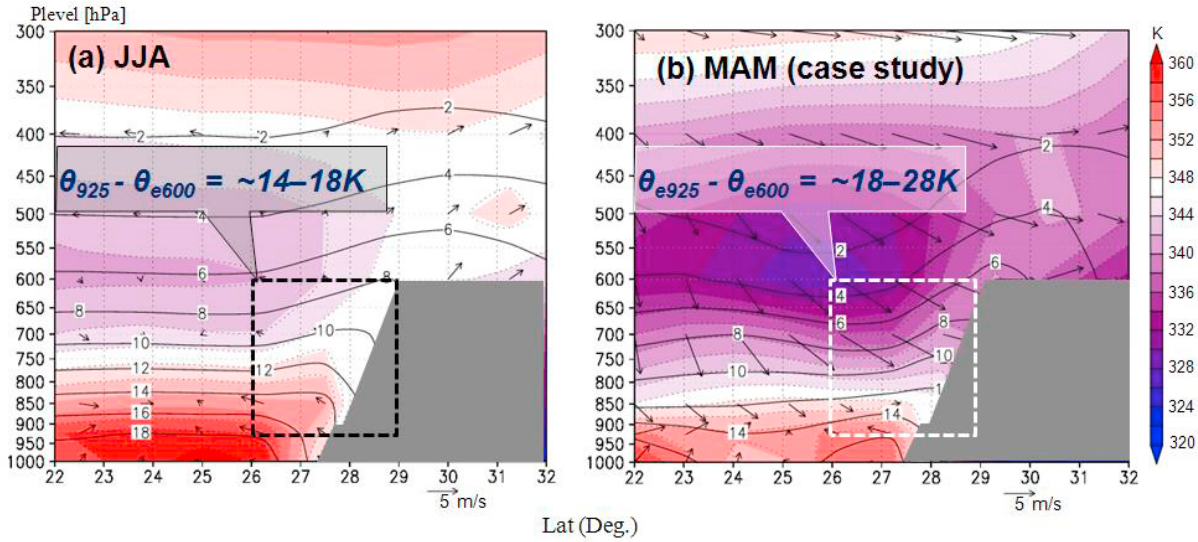

Figure 12. Height-latitude sections of equivalent potential temperature (K; color shaded), horizontal wind vector (m/s; black arrows), and specific humidity (gm/kg, contours) at 84.5°E for (a) JJA climatological mean and (b) MAM case study. White dashed rectangle and black shading roughly represents the cross section of the study area and Himalayan topography at the same location.

JRA-25 reanalysis suggested weak AI in MAM (figure not shown). During JJA, the AI was relatively strong (∼14–18 K) (Figure 12a) compared with MAM (∼10–12 K). This is consistent with the findings of *Bhatt and Nakamura* [2006]. We did not observe a strong AI in the long term climatological data during MAM, although intense rainfall was noted (Figures 5c and 7a). This is probably because of the lower number of precipitation systems. Most days were without precipitation, and only a few systems with intense rainfall developed during the late pre-monsoon seasons. Thus, we checked the vertical structure for selected rainfall events during May in 2004 (days: 16, 17, 20, 21, and 28). Daily rain totals during those days were more than 0.5σ from the average of MAM. Figure 12b shows the composite of vertical structure of atmospheric conditions (equivalent potential temperature, relative humidity, and wind vector) during those days. There appears to be a strong instability (∼18–28 K) with higher theta-e in the lower atmosphere over the southern plains and foothills of the Himalayas. Although the theta-e is higher over the southern plains, the specific humidity is lower (∼14 g/kg). This indicates that the high theta-e can be attributed to the high temperature of rather dry air. Similar characteristics were also noticed during major rainfall events in previous and successive years (figures not shown).

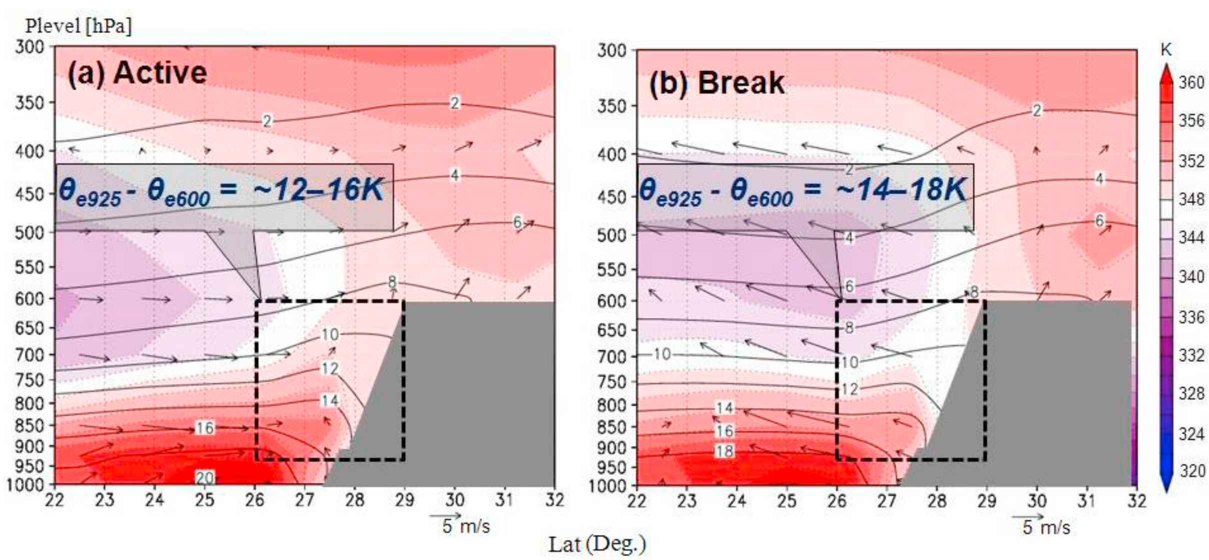

Figure 13. As in Figure 12, but for (a) active monsoon, and (b) break monsoon.

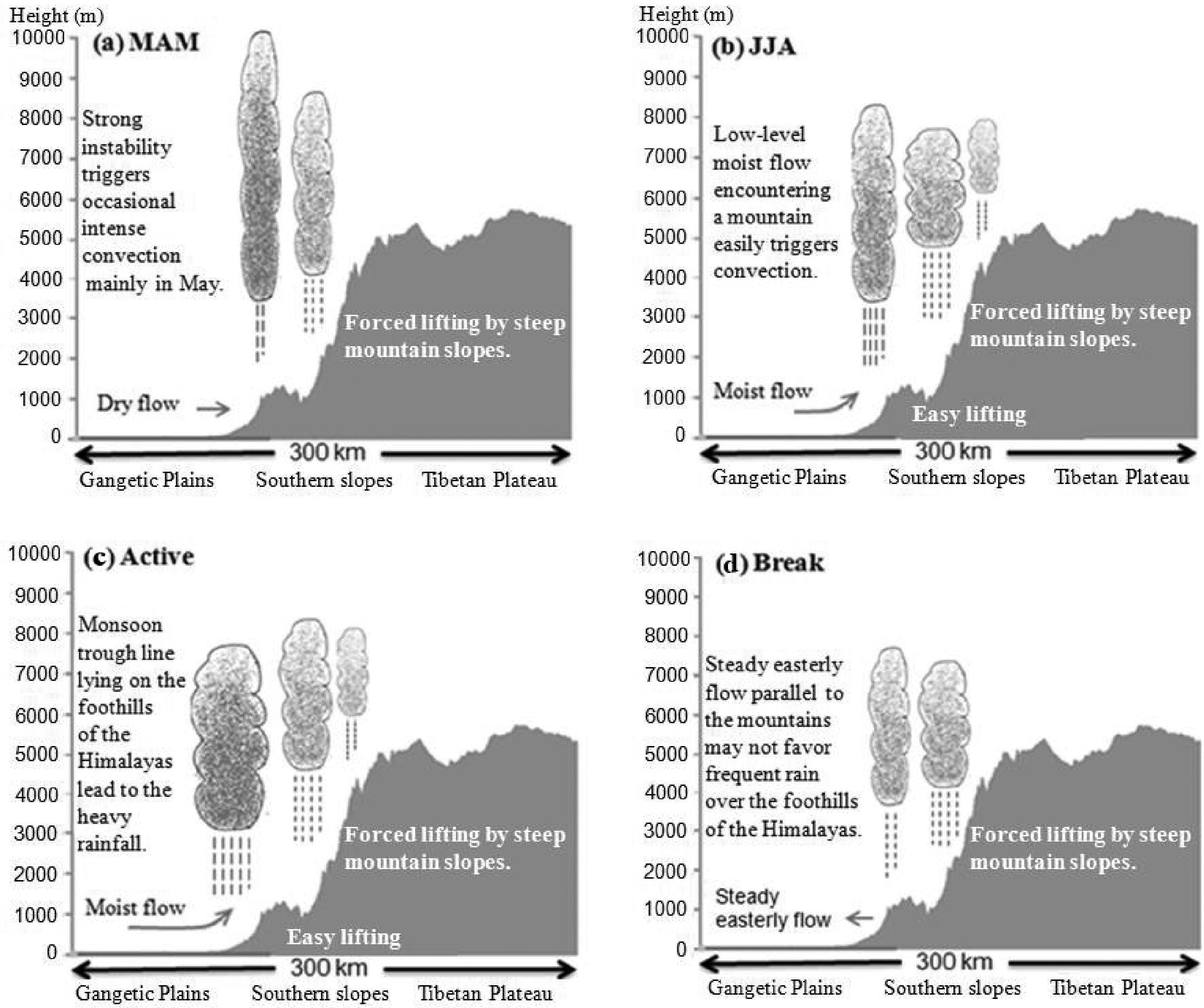

Figure 14. Schematic illustrations of spatiotemporal variation in rainfall for (a) pre-monsoon (MAM), (b) summer monsoon (JJA), (c) active monsoon, and (d) break monsoon.

[31] Now, we discuss the vertical structure of the active- and break-monsoon atmospheric conditions. Figure 13 shows the composite of vertical structure of atmospheric conditions during active and break periods for 11 years; their distributions are remarkably similar, except for the horizontal wind component. During active phases, there is weak northward wind flow close to the Himalayas from the lower to middle atmosphere (Figure 13a), but apparent easterly flow (in other words steady flow parallel to mountain ranges) in break periods (Figure 13b). These tendencies are in good agreement with low-level convergence (divergence) during active (break) periods along the Himalayan foothills (figure not shown). The difference in equivalent potential temperature ($\theta_{e925} - \theta_{e600}$) in active periods was slightly lower ($\sim$12–16 K) than that in break phases ($\sim$14–18 K), indicating higher atmospheric stability during the active monsoon. However, there is slightly more moisture in the lower atmosphere during active periods. The abundant supply of the moisture due to southeasterly flow in the active periods provides favorable conditions for generation of precipitation systems near the SH.

5. Discussions

[32] The north-south topographic gradient in the central Himalayas is extremely high, and is characterized by two-step topography [*Bookhagen and Burbank*, 2006, 2010], which can cause strong orographic forcing. Thus, variation in rainfall characteristics between the southern Himalayan foothills and higher altitudes could be pronounced. A schematic of rainfall processes over the southern slopes of the Himalayas (focusing on the CHR) during MAM and JJA (including active and break periods) is presented in Figure 14. Once precipitation systems begin, they tend to be more intense during MAM (Figure 14a) than JJA (Figure 14b). This is consistent with more intense lightning activity during MAM than JJA over the CHR [*Bhatt*, 2005; *Barros et al.*, 2004]. During MAM, the CHR is characterized by a dry atmosphere with strong dry northwesterly winds. This generally does not favor generation

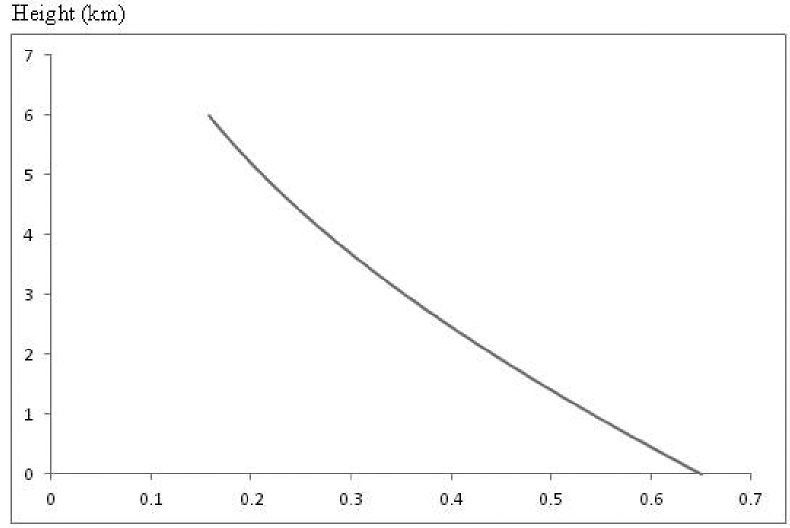

Figure 15. Amount of condensation for 1-kg air by steady lifting. The temperature lapse rate is assumed to be 6.5°C/km; air temperature and air pressure are 30°C and 1013 hPa, respectively, at 1-m height.

of precipitation systems. Despite the unfavorable synoptic conditions, rainfall is yielded from a limited amount of locally enhanced convective activity. The intense rainfall that occurs during MAM over the SH is due to strong AI (Figures 7a and 13a), that is, once convection starts, it is likely to strengthen. More precipitation systems develop over the LH than over the SH, resulting in a higher rain rate in the LH. This is probably orographically enhanced convection. In other words, strong AI triggers deep intense rain systems near the SH, whereas orography triggers frequent rain systems over the higher Himalayas. The deep convection over the SH may help moisten the middle layer and reduce atmospheric instability. During JJA, systems are less convective but more persistent with higher mean rain rate. Such rainfall characteristics may suggest that precipitation systems develop in humid and more stable environments. The important characteristics of rainfall distribution during JJA over the southern slope of the CHR are as follows: the SH peak is a result of intense rainfall, and the LH peak of persistent rainfall. This fact suggests different rainfall processes over the SH and LH. The frequent lightning events in the lower elevation areas also support the assertion that rainfall over these areas occurs with stronger convection [*Bookhagen and Burbank*, 2010]. Precipitation systems near the SH may be categorized by abundance of water vapor in the lower atmosphere, while higher Himalayan precipitation systems involve more mechanical processes (i.e., forced lifting due to steep Himalayan slopes). These features are similar to those in MAM, but the precipitation systems are generally weaker.

[33] As explained in section 4.3, the active-phase rainfall is concentrated around SH (Figure 14c); it is first attributed to conditional rain rate, followed by rain frequency. Despite the lower rain-top height (~8 km), intense rainfall appears up to 6 km elevation (Figure 10a). This means that abundant moisture supply in the lower atmosphere favors easy trigging of convection, when the moisture encounters low frontal mountains ranges; *Houze* [2012] explained such triggering over the foothills ahead of the main mountain barrier. The moisture convergence during active periods is associated with the shifting of the trough line close to the foothills of the Himalayas. Conversely, break periods are characterized by relatively lower moisture content, steady easterly winds and higher solar radiation as the monsoon trough shifts southwards. Such conditions generally do not favor ample rising of dry air to reach the lifting condensation level (LCL). Thus, rainfall systems rarely propagate over low land. Precipitation systems in break periods exist under rather unstable atmospheric conditions, enhanced by strong solar heating. Despite the lower moisture content in the air, the major mountain barrier provides a strong trigger to initiate convection over higher altitude regions (Figure 14d).

[34] One of the interesting findings is that the rain-conditioned rain rate simply decreases with altitude regardless of the rain amount in wet seasons, while the rain frequency peaks near an elevation of approximately 2,100 m (Figure 6). How can this result be understood? One idea is that the rain is caused by forced lifting. When humid air collides with the mountain slope, it is lifted along the slope. The air temperature decreases as the air lifts and, at the LCL, condensation occurs and rain begins. If the lifting continues, the rain persists. In this case, the amount of rain could simply be estimated from the change in saturation water vapor pressure with temperature. Figure 15 shows the amount of condensation relative to altitude on the basis of the hypothesis that the air is saturated at the beginning. The saturated air produces rain in proportion to the lines in the figure. When the colliding air is not saturated by water vapor, condensation will not appear below the LCL. In this case, no precipitation appears below the LCL. Actual relative humidity varies, as does the LCL. Thus, the amount of rain after averaging may peak at an elevated level instead of ground level. On the other hand, if the lifting is nearly the same under wet or dry

conditions, the rain-conditioned rain rate may be the same. Thus, the rain-conditioned rain rate monotonically decreases with elevation independently of the rain total, but the frequency of rain peaks at a specific level.

6. Conclusions

[35] This study has been performed over the rugged topography of the central Himalayas using 11-year (1998–2008) TRMM PR near-surface rainfall data, JRA-25 reanalysis data, and GTOPO30 elevation data. Spatial and temporal variations of rainfall were analyzed for pre-monsoon and summer monsoon seasons, with a particular focus on their relationship with altitude.

[36] The analysis of rainfall characteristics showed different scenarios for the spatiotemporal distribution of rainfall during the summer monsoon and pre-monsoon periods. There is an increase in peak rainfall over higher altitudes, and a decrease over the frontal low-altitude region, during the pre-monsoon season. A case study in 2004 revealed that a few intense rainfall events dominate pre-monsoon rainfall and are associated with strong atmospheric instability. During the summer monsoon, two high-rainfall zones clearly appeared over the southern slope of the central Himalayan region. The frontal high-rainfall zone coincided with the Sub-Himalayas (~500–700 m AMSL) and the inner, rather broad high-rainfall zone coincided with the Lesser Himalayas (~2,000–2,200 m AMSL). The southern slope of the Sub-Himalayas received high rainfall as a result of fewer heavy rainfall events, while the Lesser Himalayas received high rainfall as a result of the high frequency of relatively weak but persistent rainfall. It is suggested that precipitation systems are mostly triggered by strong atmospheric instability in the pre-monsoon season, while sufficient moisture induced by low-level southeasterly flow triggers persistent rainfall during the summer monsoon season.

[37] In addition, an inspection of intraseasonal variability in rainfall during the mature monsoon season revealed that active-phase rainfall was dominant over the slopes of the frontal low mountains; however, break-phase rainfall was dominant in total monsoon rainfall over the Lesser Himalayas. High temperatures and strong low-level moisture flowing over low elevations may create favorable conditions to initiate convective rainfall. Although such conditions do not appear over higher terrain, forced lifting due to steep orography favors persistent rainfall.

[38] **Acknowledgments.** The authors acknowledge H. Masunaga, members of the Laboratory of Satellite Meteorology and members of Laboratory of Cloud and Precipitation at the Hydrospheric Atmospheric Research Center for their valuable suggestions and cooperation. We are grateful to B. Bookhagen and two anonymous reviewers for thoughtful comments and suggestions. The TRMM PR data used in this study were provided by Japan Aerospace Exploration Agency (JAXA). The climatological data sets were obtained from the JRA-25 Long-term Reanalysis Cooperative Research Project conducted by the Japan Meteorological Agency (JMA) and the Central Research Institute of Electric Power Industry (CRIEPI).

References

Anders, A. H., G. H. Roe, B. Hallet, D. R. Montgomery, N. J. Finnegan, and J. Putkonen (2006), Spatial patterns of precipitation and topography in the Himalaya, *Spec. Pap. Geol. Soc. Am.*, *398*, 39–53.

Annamalai, H., and J. M. Slingo (2001), Active/break cycles: Diagnosis of the intraseasonal variability of the Asian summer monsoon, *Clim. Dyn.*, *18*, 85–102, doi:10.1007/s003820100161.

Awaka, J., T. Iguchi, and K. Okamoto (1997), Rain type classification algorithm for TRMM precipitation radar, *IEEE Trans. Geosci. Remote Sens.*, *4*, 1633–1635.

Barros, A. P., G. Kim, E. Williams, and W. Nesbitt (2004), Probing orographic controls in the Himalayas during the monsoon using satellite imagery, *Nat. Hazards Earth Syst. Sci.*, *4*, 29–51, doi:10.5194/nhess-4-29-2004.

Barros, A. P., S. Chiao, T. J. Lang, D. Burbank, and J. Putkonen (2006), From weather to climate seasonal and interannual variability of storms and implications for erosion processes in the Himalaya, *Spec. Pap. Geol. Soc. Am.*, *398*, 17–18.

Bell, T. L., and P. K. Kundu (2000), Dependence of satellite sampling error on monthly averaged rain rates: Comparison of simple models and recent studies, *J. Clim.*, *13*, 449–462, doi:10.1175/1520-0442(2000)013<0449:DOSSEO>2.0.CO;2.

Bhatt, B. C. (2005), Study on the seasonal and diurnal variation of the precipitation around the Himalayan region, doctor's thesis, Dep. of Earth and Environ. Sci., Nagoya Univ., Nagoya, Japan.

Bhatt, B. C., and K. Nakamura (2005), Characteristics of monsoon rainfall around the Himalayas revealed by TRMM precipitation radar, *Mon. Weather Rev.*, *133*, 149–165, doi:10.1175/MWR-2846.1.

Bhatt, B. C., and K. Nakamura (2006), A climatological-dynamical analysis associated with precipitation around the southern part of the Himalayas, *J. Geophys. Res.*, *111*, D02115, doi:10.1029/2005JD006197.

Bookhagen, B. (2010), Appearance of extreme monsoonal rainfall events and their impact on erosion in the Himalaya, *Geomatics Nat. Hazards Risk*, *1*, 37–50, doi:10.1080/19475701003625737.

Bookhagen, B., and D. W. Burbank (2006), Topography, relief, and TRMM-derived rainfall variations along the Himalaya, *Geophys. Res. Lett.*, *33*, L08405, doi:10.1029/2006GL026037.

Bookhagen, B., and D. W. Burbank (2010), Toward a complete Himalayan hydrological budget: Spatiotemporal distribution of snowmelt and rainfall and their impact on river discharge, *J. Geophys. Res.*, *115*, F03019, doi:10.1029/2009JF001426.

Bookhagen, B., and M. R. Strecker (2008), Orographic barriers, high-resolution TRMM rainfall, and relief variations along the eastern Andes, *Geophys. Res. Lett.*, *35*, L06403, doi:10.1029/2007GL032011.

Boos, W. R., and Z. Kuang (2010), Dominant control of the South Asian monsoon by orographic insulation versus plateau heating, *Nature*, *463*, 218–222, doi:10.1038/nature08707.

Chater, A. M., and A. P. Sturman (1998), Atmospheric conditions influencing the spillover of rainfall to lee of the southern Alps, New Zealand, *Int. J. Climatol.*, *18*, 77–92, doi:10.1002/(SICI)1097-0088(199801)18:1<77::AID-JOC218>3.0.CO;2-M.

Dairaku, K., S. Emori, and T. Oki (2004), Rainfall amount, intensity, duration and frequency relationships in the Mae Cheam watershed in Southeast Asia, *J. Hydrometeor*, *5*, 458–470, doi:10.1175/1525-7541(2004)005<0458:RAIDAF>2.0.CO;2.

Dhar, O. N., and P. R. Rakhecha (1981), The effect of elevation on monsoon rainfall distribution in the central Himalayas, in *Monsoon Dynamics*, edited by J. Lighthill and R. P. Pearce, pp. 253–260, Cambridge Univ. Press, Cambridge, U. K.

Dhar, O. N., M. K. Soman, and S. S. Mulye (1984), Rainfall over the southern slopes of the Himalayas and the adjoining plains during "breaks" in the monsoon, *J. Climatol.*, *4*, 671–676, doi:10.1002/joc.3370040610.

Engman, E. T., and D. M. Hershfield (1969), Precipitation climatology of the Sleepers River watershed near Danville, Vermont, *U. S. Dep. Agric., Agric. Res. Serv.*, *41–148*, 22 pp .

Flohn, H. (1957), Large-scale aspects of the "summer monsoon" in south and East Asia, *J. Meteorol. Soc. Jpn.*, *75*, 180–186.

Gadgil, S., and P. V. Joseph (2003), On breaks of the Indian monsoon, *Proc. Indian Acad. Sci.*, *112*, 529–558.

Goswami, B. N., and R. S. Ajaya Mohan (2001), Intraseasonal oscillations and interannual variability of the Indian summer monsoon, *J. Clim.*, *14*, 1180–1198, doi:10.1175/1520-0442(2001)014<1180:IOAIVO>2.0.CO;2.

Houze, R. A. (2012), Orographic effects on precipitating clouds, *Rev. Geophys.*, *50*, RG1001, doi:10.1029/2011RG000365.

Houze, R. A., D. C. Wilton, and B. F. Smull (2007), Monsoon convection in the Himalayan region as seen by the TRMM precipitation radar, *Q. J. R. Meteorol. Soc.*, *133*, 1389–1411.

Huffman, G. J., et al. (2007), The TRMM multi-satellite precipitation analysis: Quasi-global, multi-year, combined-sensor precipitation estimates at fine scales, *J. Hydrometeorol.*, *8*, 38–55, doi:10.1175/JHM560.1.

Iguchi, T., T. Kozu, R. Meneghini, J. Awaka, and K. Okamoto (2000), Rain-profiling algorithm for the TRMM Precipitation Radar, *J. Appl. Meteorol.*, *39*, 2038–2052.

Krishnamurthy, V., and J. Shukla (2000), Intra-seasonal and inter-annual variations of rainfall over India, *J. Clim.*, *13*, 4366–4377, doi:10.1175/1520-0442(2000)013<0001:IAIVOR>2.0.CO;2.

Krishnan, R., C. Zhang, and M. Sugi (2000), Dynamics of breaks in the Indian summer monsoon, *J. Atmos. Sci.*, *57*, 1354–1372, doi:10.1175/1520-0469(2000)057<1354:DOBITI>2.0.CO;2.

Kummerow, C., W. Barnes, T. Kozu, J. Shiue, and J. Simpson (1998), The Tropical Rainfall Measuring Mission (TRMM) sensor package, *J. Atmos. Oceanic Technol.*, *15*, 809–817, doi:10.1175/1520-0426(1998)015<0809:TTRMMT>2.0.CO;2.

Kummerow, C., et al. (2000), The status of Tropical Rainfall Measuring Mission (TRMM) after two years in orbit, *J. Appl. Meteorol.*, *39*, 1965–1982, doi:10.1175/1520-0450(2001)040<1965:TSOTTR>2.0.CO;2.

Linsley, R. K., M. A. Kohler, and J. L. H. Paulhus (1949), *Applied Hydrology*, Mc Graw Hill, New York.

Nayava, J. L. (1980), Rainfall in Nepal: The Himalayan review, *Nepal Geogr. Soc.*, *12*, 1–18.

Nesbitt, S. W., and E. J. Zisper (2003), The diurnal cycle of rainfall and convective intensity according to three years of TRMM measurements, *J. Clim.*, *16*, 1456–1475, doi:10.1175/1520-0442-16.10.1456.

Onogi, K., et al. (2005), JRA-25: Japanese 25-year Re-analysis project–progress and status, *Q. J. R. Meteorol. Soc.*, *131*, 3259–3268, doi:10.1256/qj.05.88.

Rajeevan, M., S. Gadgil, and J. Bhate (2010), Active and break spells of the Indian summer monsoon, *J. Earth Syst. Sci.*, *119*, 229–247, doi:10.1007/s12040-010-0019-4.

Ramamurthy, K. (1969), Monsoon of India: Some aspects of the "break" in the Indian southwest monsoon during July and August, *Forcasting Man. 18.3*, 57 pp., Indian Meteorol. Dep., Poona, India.

Romatschke, U., and R. A. Houze (2011a), Characteristics of precipitating convective systems in the South Asian monsoon, *J. Hydrometeorol.*, *12*, 157–180, doi:10.1175/2010JHM1311.1.

Romatschke, U., and R. A. Houze (2011b), Characteristics of precipitating convective systems in the premonsoon season of South Asia, *J. Hydrometeorol.*, *12*, 3–26, doi:10.1175/2010JHM1289.1.

Rumley, J. B. (1965), An investigation of the distribution of rainfall with the elevation for selected station in Ecuador, master's thesis, Texas A & M Univ., College Station.

Shrestha, M. L. (2000), Interannual variation of summer monsoon rainfall over Nepal and its relation to southern oscillation index, *Meteorol. Atmos. Phys.*, *75*, 21–28, doi:10.1007/s007030070012.

Singh, P., and N. Kumar (1997), Effect of orography on precipitation in the western Himalayan region, *J. Hydrol.*, *199*, 183–206, doi:10.1016/S0022-1694(96)03222-2.

Singh, P., and K. Nakamura (2010), Diurnal variation in summer monsoon precipitation during active and break periods over central India and southern Himalayan foothills, *J. Geophys. Res.*, *115*, D12122, doi:10.1029/2009JD012794.

Singh, P., K. S. Ramasastri, and N. Kumar (1995), Topographical influence on precipitation distribution in different ranges of western Himalayas, *Nord. Hydrol.*, *26*, 259–284.

Sokol, Z., and V. Bližňák (2009), Areal distribution and precipitation–altitude relationship of heavy short-term precipitation in the Czech Republic in the warm part of the year, *Atmos. Res.*, *94*, 652–662, doi:10.1016/j.atmosres.2009.03.001.

Steiner, M., R. A. Houze Jr., and S. E. Yuter (1995), Climatological characterization of three-dimensional storm structure from operational radar and rain gauge data, *J. Appl. Meteorol.*, *34*, 1978–2007, doi:10.1175/1520-0450(1995)034<1978:CCOTDS>2.0.CO;2.

Suprit, K., and D. Shankar (2008), Resolving orographic rainfall on the Indian West Coast, *Int. J. Climatol.*, *28*, 643–657, doi:10.1002/joc.1566.

Takahashi, H. G., H. Fujinami, T. Yasunari, and J. Matsumoto (2010), Diurnal rainfall pattern observed by Tropical Rainfall Measuring Mission Precipitation Radar (TRMM-PR) around the Indochina peninsula, *J. Geophys. Res.*, *115*, D07109, doi:10.1029/2009JD012155.

Webster, P. J., V. O. Magana, T. N. Palmer, J. Shukla, R. A. Tomas, M. Yanai, and T. Yasunari (1998), Monsoons: Process, predictability, and the prospects for prediction, *J. Geophys. Res.*, *103*, 14,451–14,510, doi:10.1029/97JC02719.